Journal of Materials Chemistry A

Accepted Manuscript

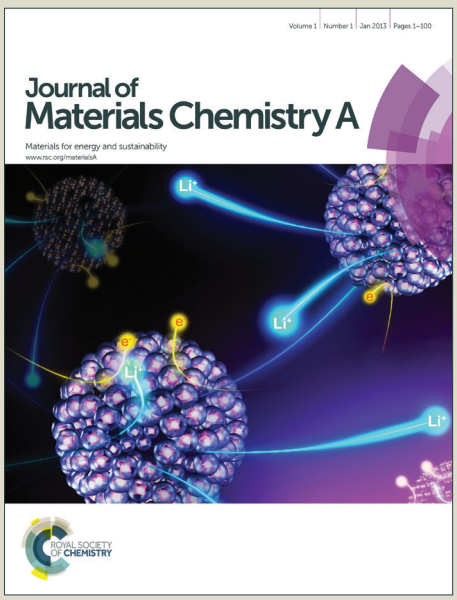

ROYAL SOCIETY OF CHEMISTRY

www.rsc.org/materialsA

Palladium Nanoparticles Incorporated within Sulfonic Acid-Functionalized MIL–101(Cr) for Efficient Catalytic Conversion of Vanillin

Fumin Zhang,*[ab] Yan Jin,[a] Yanghe Fu,[a] Yijun Zhong,[a] Weidong Zhu,[a] Amr Awad Ibrahim,[b] and M. Samy El-Shall*[b]

[a] Key Laboratory of the Ministry of Education for Advanced Catalysis Materials, Institute of Physical Chemistry, Zhejiang Normal University, 321004 Jinhua, People's Republic of China

[b] Department of Chemistry, Virginia Commonwealth University 23284 Richmond, VA, United States

ABSTRACT

We report a highly efficient bifunctional catalyst, Pd/SO_3H-MIL–101(Cr), consisting of Pd nanoparticles immobilized on a mesoporous sulfonic acid-functionalized metal–organic framework SO_3H-MIL–101(Cr), which exhibits high catalytic performance in promoting biomass refining. The use of SO_3H-MIL–101(Cr) as a support renders highly dispersed Pd nanoparticles with uniform size distribution, sufficient reactants contact in aqueous media, and rapid activation of the reactants induced by the Brønsted acid coordination sites (sulfonic acid groups from SO_3H-MIL–101(Cr)). Thus, the 2.0 wt.% Pd/SO_3H-MIL–101(Cr) catalyst exhibits novel synergy in the hydrodeoxygenation of vanillin (a typical model compound of lignin) at low H_2 pressure under mild conditions in aqueous media. Excellent catalytic results (100% conversion of vanillin with exclusive selectivity for the 2-methoxy-4-methylphenol product) could be achieved, and no loss of catalytic activity and selectivity were observed after seven recycles in succession.

KEYWORDS: Metal–organic frameworks; Sulfonic acid-functionalized MIL–101(Cr); Pd nanoparticles; Hydrodeoxygenation; Vanillin

Corresponding Authors:

E-mail: zhangfumin@zjnu.edu.cn, fzhang5@vcu.edu (F. Zhang).
Tel.: +86 579 822-88919; Fax: +86 579 82282234

E-mail: mselshal@vcu.edu (M. Samy El-Shall).
Tel.: +1 804 828-3518; Fax: +1 804 828-8599

1. Introduction

Growing worldwide energy demand, high commodity prices, high economic growth, and growing scientific evidence that atmospheric carbon dioxide is among the most important contributors to global climate change make it urgent to increase energy supply and reduce worldwide greenhouse gas emissions at the same time [1-3]. Increasing energy supply requires efficient energy production and expanded development of alternative sources of energy. Biomass is a renewable resource and, if properly produced and catalytically converted, can yield both biofuels that have lower greenhouse gas emissions than petroleum-based gasoline and diesel as well as high-value chemical products such as phenols that can be directly used in the chemical and pharmaceutical industries [4-6].

Lignocellulosic biomass feedstocks are a complex mixture of three structural biopolymers (lignin, cellulose and hemicellulose) and minor non-structural components [7]. Unlike fossil hydrocarbons of petroleum or natural gas feedstocks, the biopolymers are oxygenated complex macromolecules and except for cellulose, there are no uniform repeating units in lignin and hemicellulose. Compared to cellulose and hemicellulose, lignin, which constitutes approximately 30 wt.% of woody biomass, is much more challenging to convert due to its highly complex structure, which consists of oxygen-rich subunits derived from phenol, *p*-coumaryl, coniferyl, and sinapyl alcohols typically connected with ether linkages [8-10]. Accordingly, it is more difficult to upgrade lignin-derived pyrolysis oil than cellulose-derived pyrolysis oil [11,12].

Heterogeneous catalytic hydrodeoxygenation is considered to be the most important and feasible strategy for bio-oil upgrading, in which supported catalysts are frequently used [13-17]. Among the various supports, activation carbon, metal oxides (e.g. TiO_2, MgO, CeO_2, γ-Al_2O_3), zeolites, SiO_2, and carbon nanotubes are frequently applied [18-23]. However, many of these supports may suffer from poor dispersion of the nanoparticle catalysts, weak catalyst-support interaction, poor water dispersibility, or reaction monofunctionality. Recently, hybrid materials have been developed as a catalyst support with enhanced catalytic performances [24-27]. For example, Wang and co-workers found that the N-doped carbon-supported Pd catalyst exhibits high activity in the hydrodeoxygenation of vanillin (4-hydroxy-3-methoxy-benzaldehyde, a typical model compound of lignin). The high

catalytic performance of this catalyst is attributed to the structure of the N-doped carbon-metal heterojunction, which leads to stable and uniform dispersion of Pd nanoparticles but also to additional electronic activation of the metal nanoparticles in the reaction medium [24]. Xiao and co-workers reported that the hydrophilic mesoporous sulfonated melamine-formaldehyde resin (MSMF)-supported Pd catalyst is highly active for the hydrodeoxygenation of vanillin, and the superior catalytic performance is attributed to the good wettability of the reactant on the Pd/MSMF catalyst [25]. In addition, Zhou and co-workers investigated the effects of the wettability of the carbonaceous microspheres-supported Pd catalysts on the performances in the hydrodeoxygenation of vanillin, and found that in the aqueous media, the more hydrophilic the catalyst, the more active it was for the hydrodeoxygenation of vanillin [26]. Obviously, the nature and surface structure of the support plays a significant role in achieving excellent catalytic hydrodeoxygenation performance.

The field of Metal–Organic Frameworks (MOFs) has provided a new class of highly porous crystalline materials with well-defined cavities or channels that can accommodate a variety of guest species of different sizes and shapes for a variety of applications in gas storage, separation and heterogeneous catalysis [27-29]. The interest in MOFs arises from their well-ordered crystalline structure, high porosity, tunable pore size, and modifiable surface properties [30-32]. Among the well-studied MOFs, the chromium-based MIL–101 possesses several unique features such as a crystal structure consisting of two quasi–spherical mesoporous cages (2.9 and 3.4 nm, respectively), extremely large surface area, numerous unsaturated metal cation sites, and high stability in water [33]. The combination of these features makes MIL–101 a unique candidate for gas storage, drug delivery, adsorptive separation, and heterogeneous catalysis [34-45].

Following the pioneering work of Kitagawa and co-workers [34], Zhang and co-workers reported a one-pot hydrothermal synthesis of a sulfonic acid-functionalized MIL–101(Cr) catalyst [SO_3H-MIL–101(Cr)] which showed superior catalytic properties in a series of esterification and acetalization reactions attributed to the accessible Brønsted acidic sites distributed throughout the framework as well as the large mesoporous cages, thus facilitating

the transfer of substrates [46,47].

In the present work, we take advantage of the unique properties of SO_3H-MIL–101(Cr) by encapsulating Pd nanoparticles within the mesoporous cages of SO_3H-MIL–101(Cr) to develop an efficient catalyst for the catalytic hydrodeoxygenation of vanillin as a model system to explore the hydrogenation and deoxygenation routes of lignin as described in Scheme 1 below.

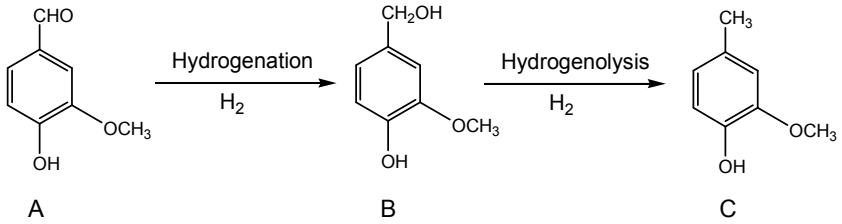

Scheme 1. Possible reaction pathways for hydrodeoxygenation of vanillin (A) to 2-methoxy-4-methyl phenol (C).

The rational design of the bifunctional Pd/SO_3H-MIL–101(Cr) catalyst is based on several considerations. First, the SO_3H-MIL–101(Cr) framework can be well dispersed in the reaction medium due to its hydrophilic properties [48], thus facilitating the adsorption and diffusion of the reactants in polar reaction medium, where Pd nanoparticles activate H_2 and promote the hydrogenation of vanillin to form 4-hydroxymethyl-2-methoxyphenol. On the other hand, the presence of acidic SO_3H moieties may accelerate further deoxygenation to produce the desired 2-methoxy-4-methyl phenol product [49]. Thus, the multifunctional catalyst system would show novel synergy in the hydrodeoxygenation of vanillin, leading to significantly enhanced catalytic properties.

2. Experimental

2.1. Chemicals

All reagents with AR purity (analytical reagent grade) were purchased and used as received without further purification. Terephthalic acid and 2-sulfoterephthalic acid

monosodium salt were purchased from J&K Scientific Ltd. Chromium nitrate monohydrate, chromium trioxide, hydrofluoric acid, hydrochloric acid (37 wt.%), methanol, ethanol, vanillin, vanillin alcohol and 2-methoxy-4-methylphenol were purchased from Sinopharm Chemical Reagent Co. Ltd. Hydrogen with a purity over 99.999% was purchased from Shanghai Pujiang Special Gas Co., Ltd. Coconut shell-based activated carbon (C in abbreviation) was kindly provided by Fujian Xinsen Carbon Corp., Ltd. Deionized water with resistance larger than 18.2 MΩ was obtained from a Millipore Milli-Q ultrapure water purification system.

2.2. Catalyst Preparation

The one-pot synthesis of sulfonic acid-functionalized MIL–101(Cr) was based on the following procedure: 2.5 g of CrO_3, 6.7 g of 2-sulfoterephthalic acid monosodium salt, and 16 mmol of HF (40 wt.%) were mixed with 25 ml of deionized water and stirred for 15 min at room temperature. The solution was then transferred into a Teflon-lined stainless steel autoclave. The synthesis was conducted without agitation in an oven at 180 °C for 24 h. The obtained green microcrystalline powder was treated in a mixed solution of diluted HCl (0.08 M) in methanol and water, and was further treated in methanol and water to remove additional HCl. Afterward; the solid was dried in a vacuum desiccator at 150 °C for 6 h prior to further analysis or use. The resulting sulfonic acid-functionalized MIL–101(Cr) was referred to as SO_3H-MIL–101(Cr). Pure MIL–101(Cr) was synthesized following the procedure reported in the literature [33].

To introduce Pd nanoparticles into MIL–101(Cr), an incipient-wetness impregnation method was applied according to the procedure described in our previous work [41]. In a typical procedure, 0.0584 g of $Pd(acac)_2$ was dissolved into 0.90 ml of chloroform with stirring and the solution was then added dropwise into 1.0 g of SO_3H-MIL–101(Cr) having a pore volume of 0.90 $cm^3\ g^{-1}$ as determined by the N_2 adsorption isotherm at −196 °C. The formed precursor catalyst was aged overnight at room temperature. Afterwards, the sample was further dried at 150 °C for 5 h in a vacuum desiccator. Finally, the dried precursor catalyst was treated in a fixed-bed stainless steel reactor with an inner diameter of 6 mm under a mixture flow containing 10 vol.% H_2 in Ar with a total flow rate of 30 ml min^{-1} and

maintained at 200 °C for 4 h to obtain 2.0 wt.% Pd/SO_3H-MIL-101(Cr). For comparison, 2.0 wt.% Pd/MIL–101(Cr) and 2.0 wt.% Pd/C catalysts were also prepared by the incipient-wet impregnation method.

2.3. Catalyst Characterization

The X-ray powder diffraction (XRD) patterns were obtained on a Philips PW3040/60 diffractometer, using Cu$K\alpha$ radiation (λ = 0.1541 nm) in a scanning range of 1.5~50° at a scanning rate of 1°min^{-1}.

N_2 adsorption isotherms were obtained at -196 °C using a Micromeritics ASAP 2020 instrument. The samples were outgassed under vacuum at 150 °C for 10 h, prior to the adsorption measurements. The pore size distribution curves were determined based on Density Functional Theory (DFT).

The Pd content in the Pd/SO_3H-MIL-101(Cr) catalyst was measured by an IRIS Intrepid II XSP inductively coupled plasma-atomic emission spectrometer (ICP-AES).

Scanning electron microscopy (SEM) was performed using Hitachi S-4800 apparatus on a sample powder previously dried and sputter-coated with a thin layer of gold. Energy-dispersive X-ray spectroscopy (EDX) analyses were also performed to confirm the presence and the distribution of Pd nanoparticles.

Transmission electron microscopy (TEM) was carried out on a JEOL JEM-1200 operating at 300 kV. The sample was diluted in ethanol to give a 1 : 5 volume ratio and sonicated for 10 min. The ethanol slurry was then dropped onto a Cu grid covered with a thin film of carbon.

The surface electronic states were investigated by X-ray photoelectron spectroscopy (XPS, Thermo VG ESCALAB250 using Al$K\alpha$ radiation). Prior to the XPS measurements, the samples were treated in a 10 vol.% H_2/Ar flow at 200 °C for 4 h. The XPS data were internally calibrated, fixing the binding energy of C 1s at 284.6 eV.

Infrared (IR) spectra were collected on a Nicolet NEXUS670 Fourier transform IR spectrophotometer in KBr disks at room temperature.

The water (or vanillin) droplet contact angles were measured at ambient temperature on a self-supporting pressed sample disc by a contact angle measuring system, Dataphysics

OCA20. Once a drop of water was deposited on the surface of the sample disc, the contact angle was determined from pictures within 3 s captured using a high performance charge-coupled-device camera.

2.4. Catalytic Reaction

The catalytic hydrodeoxygenation of vanillin was carried out in a 50 ml Teflon-lined autoclave equipped with stirrer, heater, and sample port. In a typical experiment, 2 mmol of vanillin, 0.05 g of catalyst, and 20 ml water as solvent were charged into the autoclave and were repeatedly purged with hydrogen gas at room temperature. Afterwards, the autoclave was heated to 100 ºC and then pressurized with hydrogen up to 0.5 MPa. Finally, the agitation was initiated with a stirring speed of 1000 rpm. A steady pressure was maintained throughout the reaction period. The mixture was extracted with ethyl acetate and the catalyst was taken out from the system by centrifugation before being analyzed by GC (Agilent 6820) equipped with an FID detector and a capillary column (DB-5, 30 m × 0.45 mm × 0.42 μm). Additionally, the reaction conditions with respect to temperature, time, hydrogen pressure, and molar ratio of the catalyst amount to vanillin were studied. In order to test the catalytic reusability of 2.0 wt.% Pd/SO_3H-MIL–101(Cr), after the reaction, the catalyst was separated by filtration, washed with ethanol, and dried in a vacuum desiccator at 150 ℃ for 5 h, and then the recovered catalyst was used in the next reaction run.

3. Results and Discussion

3.1. Catalyst Characterization

The low-angle powder XRD pattern of the prepared SO_3H-MIL–101(Cr) (Fig. 1) matches well with that of the pristine MIL-101(Cr) reported by Férey *et al* [33], and no apparent loss of crystallinity in the XRD pattern was observed upon introduction of the sulfonic acid groups on the framework of MIL-101(Cr). After the incorporation of Pd nanoparticles, the structure of SO_3H-MIL–101(Cr) is well preserved for the 2.0 wt.% Pd/SO_3H-MIL–101(Cr) catalyst. Additionally, no significant diffraction peak ascribed to Pd species is observed for 2.0 wt.% Pd/SO_3H-MIL–101(Cr) catalyst from the wide-angle XRD pattern (Fig. S1), indicating that the Pd nanoparticles are well dispersed on the support. TEM

images demonstrate that the Pd nanoparticles are well dispersed within the SO_3H-MIL–101(Cr) with a uniform size of 3.0 ± 0.6 nm as shown in Fig. 2. EDX analyses also confirm that the Pd nanoparticles are evenly dispersed within SO_3H-MIL–101(Cr) as shown in Fig. 3.

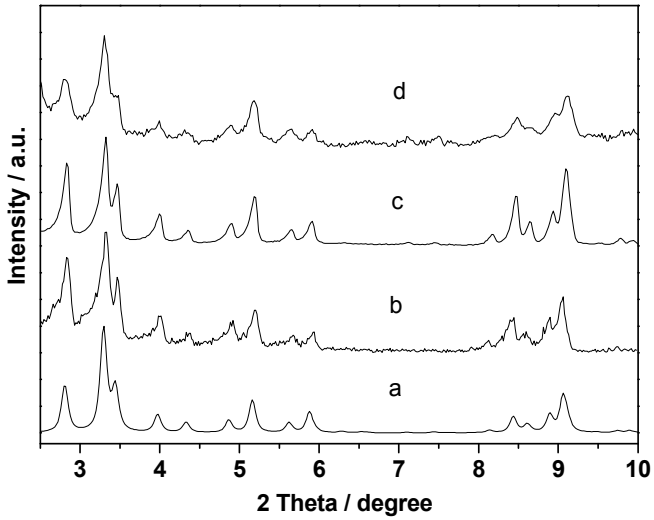

Fig. 1. Low-angle XRD patterns of MIL–101(Cr) simulated from crystal structure data (a), SO_3H-MIL–101(Cr) (b), the refresh 2.0 wt.% Pd/SO_3H-MIL–101(Cr) (c), and the used 2.0 wt.% Pd/SO_3H-MIL–101(Cr) (d).

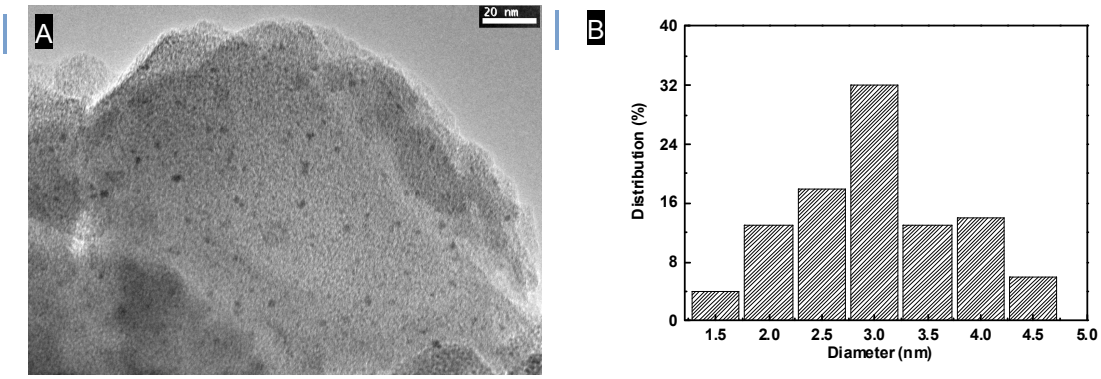

Fig. 2. TEM image of 2.0 wt.% Pd/SO_3H-MIL–101(Cr) (A) and the corresponding size distribution plot of Pd nanoparticles (B).

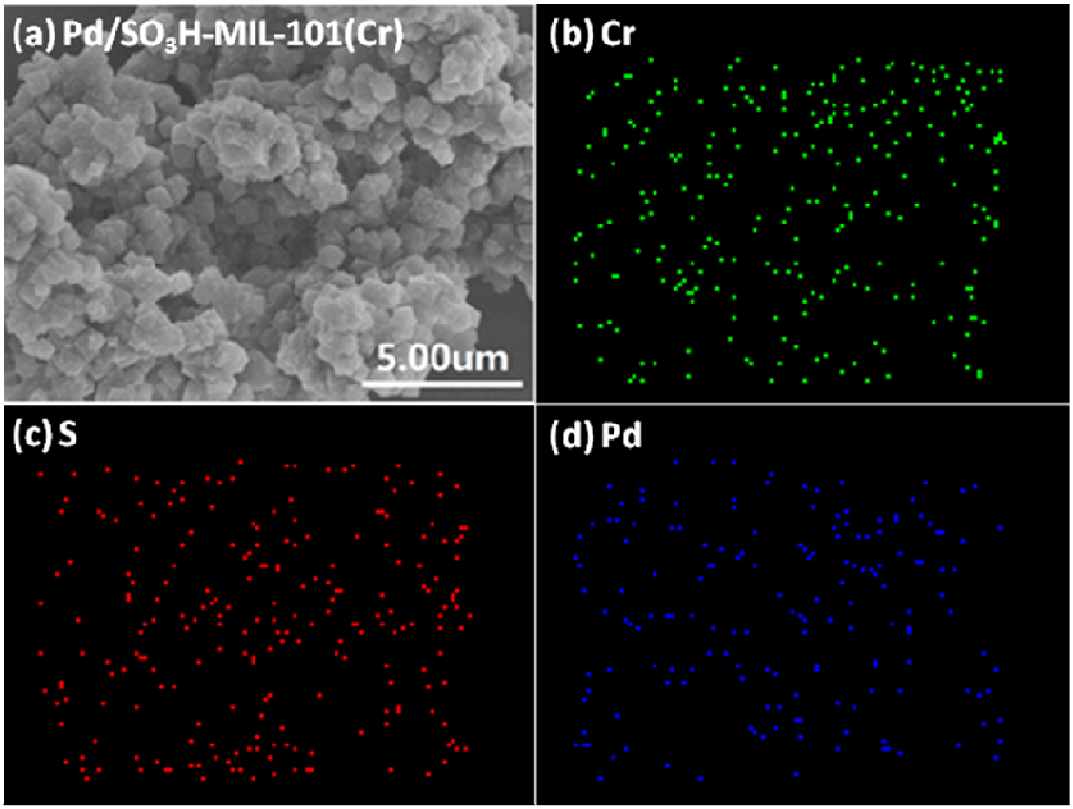

Fig. 3. SEM and EDS analysis of 2.0 wt.% Pd/SO_3H-MIL–101(Cr).

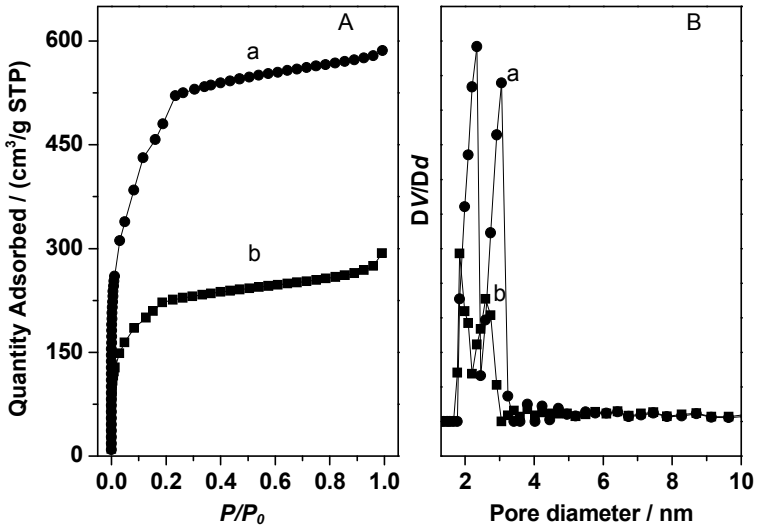

Fig. 4. N_2 isotherms at –196 °C (A) and DFT pore size distributions (B) of SO_3H-MIL–101(Cr) (a) and 2.0 wt.% Pd/SO_3H-MIL–101(Cr) (b).

N_2 gas sorption isotherms at –196 ^oC (Fig. 4 and Table S1) reveal that SO_3H-MIL–101(Cr) and 2.0 wt.% Pd/SO_3H-MIL–101(Cr) have BET specific surface areas of 1754 and 820.3 m^2 g^{-1}, respectively. The DFT pore size distribution curve of 2.0 wt.% Pd/SO_3H-MIL–101(Cr) decreases slightly in size compared with those of the parent SO_3H-MIL–101(Cr) (Fig. 4B), implying that the introduction of Pd nanoparticles can partially occupy the cages of SO_3H-MIL–101(Cr).

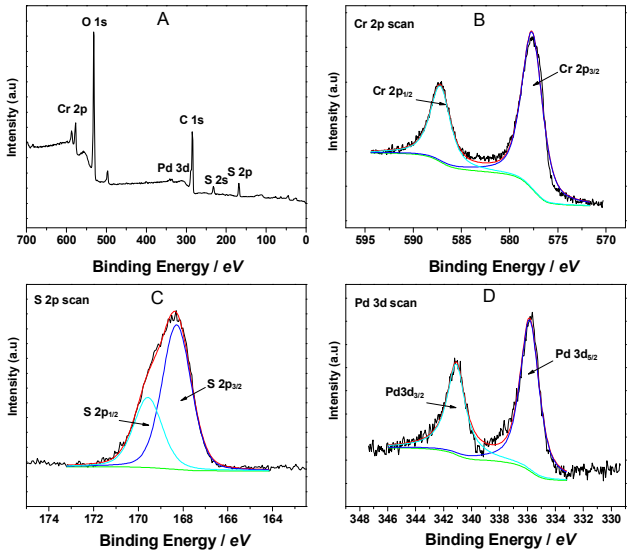

Fig. 5. XPS spectra of 2.0 wt.% Pd/SO_3H-MIL–101(Cr): survey spectrum (A), high resolution of Cr spectrum (B), high resolution of S spectrum (C), and high resolution of Pd spectrum (D).

Fig. 5A shows the survey XPS data and indicates that 2.0 wt.% Pd/SO_3H-MIL–101(Cr) contained five elements Cr, O, C, S, and Pd. The S 2p spectrum of the catalyst shows two different peaks (Fig. 5C), which can be attributed to the S–O (168.7 eV) and S=O bonds (169.9 eV) at an intensity ratio of 1:2 with a peak separation of 1.2 eV [47]. These two bonds indicate that the S in 2.0 wt.% Pd/SO_3H-MIL–101(Cr) is mainly in the form of SO_3H groups bonded to the MIL–101(Cr) framework [47]. The sample exhibits Pd $3d_{5/2}$ bands at *ca*. 335.8 and 341.4 eV, respectively, typical for metallic Pd [41], implying that the Pd(II) cations in the precursor catalyst could be reduced to Pd(0) by hydrogen. The FT-IR bands related to the sulfonic acid groups are well observed in bands ranging from 600 cm^{-1} and 1400 cm^{-1} for

both of SO_3H-MIL–101(Cr) and 2.0 wt.% Pd/SO_3H-MIL–101 (Fig. S2) [46,47].

Fig. 6 shows the contact angles of water and vanillin on the surface of 2.0 wt.% Pd/SO_3H-MIL–101(Cr) and Pd/C catalysts. It was observed that the water and vanillin droplets could be immediately adsorbed within the framework of 2.0 wt.% Pd/SO_3H-MIL–101(Cr), forming a swollen surface (Fig. 6A and 6B). The hydrophilic properties for 2.0 wt.% Pd/SO_3H-MIL–101(Cr) are probably derived from the highly hydrophilic character of the MIL–101(Cr) frameworks [48]. Considering that vanillin and vanillin alcohol are highly soluble in the aqueous phase, the hydrophilic properties of the 2.0 wt.% Pd/SO_3H-MIL–101(Cr) catalyst are anticipated to increase the catalytic efficiency in the hydrodeoxygenation reaction by the enrichment of the organic substance on the catalyst surface. On the other hand, the sulfonic acid groups from SO_3H-MIL–101(Cr) would also favor the adsorption and activation of vanillin and vanillin alcohol due to the interaction between the aromatic substrate and the acidic sites [47]. The mechanisms of Brønsted acid catalysis as well as the synergy between metal and Brønsted acid in the field of organocatalysis have been discussed in the comprehensive review by *Rueping et al* [50]. Accordingly, the hydrodeoxygenation of vanillin, as a sequential reaction catalyzed by the bifunctional catalyst combined Pd nanoparticles and Brønsted acid sites, can be explained by the two step reactions shown in Scheme 1. In the first step, vanillin is hydrogenated by the Pd nanoparticles to form vanillin alcohol, in which the catalytic activity is mainly related to the particle size of the Pd nanoparticles. Afterwards, hydrogenolyis of vanillin alcohol to 2-methoxy-4-methylphenol is triggered by the combination of Pd nanoparticles and Brønsted acid sites, in which the role of Brønsted acid sites are to activate the vanillin alcohol by forming an ion pair intermediate [50].

While the product resulting from hydrogenolysis of vanillin is much more hydrophobic and insoluble in water [27], which is more valuable as a fuel component, it is easily desorbed from the active sites and can be readily incorporated in the product stream. In contrast, when a water droplet is in contact with the Pd/C catalyst, the contact angle is as high as 46^o (Fig 6B), indicating that the Pd/C catalyst exhibits more hydrophobic character in comparison with that of the 2.0 wt.% Pd/SO_3H-MIL–101(Cr) catalyst. On the other hand, when a vanillin droplet is in contact with the surface of 2.0 wt.% Pd@SO_3H-MIL–101(Cr), the angle is as

low as 9.5° (Fig. 5D). The adsorption mechanism of vanillin droplets into 2.0 wt.% Pd/SO_3H-MIL–101(Cr) and Pd/C is probably based on the principle of the dissolution in the similar material structure. These results suggest that the Pd/C catalyst has a poorer water wettability than the 2.0 wt.% Pd/SO_3H-MIL–101(Cr) catalyst. The combination of the results from XRD, SEM, TEM, N_2 adsorption, XPS, FT-IR and the contact angle characterizations, leads to the conclusion that the sulfonic acid-functionalized MIL–101(Cr) immobilized Pd catalyst with large surface area (820 m^2 g^{-1}), small well-dispersed Pd nanoparticles (3-4 nm) and high hydrophilic character has been successfully prepared.

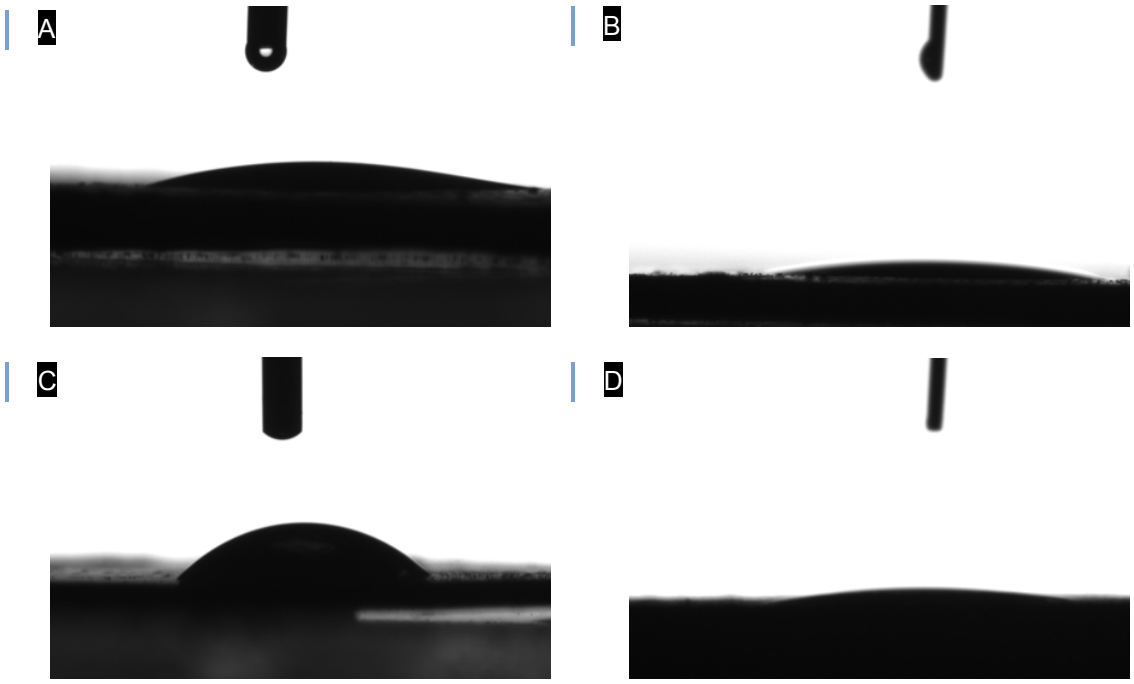

Fig. 6. Contact angles of water droplets on (A) 2.0 wt.% Pd/SO_3H-MIL–101(Cr) and (C) 2.0 wt.% Pd/C and vanillin droplets on (B) 2.0 wt.% Pd@SO_3H-MIL–101(Cr) and (D) 2.0 wt.% Pd/C.

3.2. Catalytic Hydrodeoxygenation of Vanillin

Considering that water is a desirable solvent for chemical reactions due to its environmentally friendly nature, low cost and easy handing, we first conducted the reaction in water and found that excellent results for the selective hydrodeoxygenation could be

achieved over the 2.0 wt.% Pd/SO_3H-MIL–101(Cr) catalyst including a 100% conversion of vanillin with a 100% selectivity for the 2-methoxy-4-methylphenol product within 120 min (entry 3 in Table 1). While in the presence of 2.0 wt.% Pd/MIL–101(Cr) catalyst, a rather low catalytic activity and selectivity were obtained when the reaction was carried out at the same conditions (entry 4). This is probably due to the lower acid strength of the MIL–101(Cr) as compared to that of the SO_3H-MIL–101(Cr) support. Over the pure support SO_3H-MIL–101(Cr) or MIL–101(Cr), however, no reaction took place, implying that Pd nanoparticles are inevitable for the vanillin hydrodeoxygenation (entries 1 and 2). Moreover, the 2.0 wt.% Pd/SO_3H-MIL–101(Cr) catalyst was also compared with the commercially available Pd/C catalyst under the same conditions. The textural properties of the 2.0 wt.% Pd/C are shown in Table S1. The loading amounts of Pd within the Pd/SO_3H-MIL–101(Cr), Pd/MIL–101(Cr) and Pd/C catalysts, determined by the ICP-AES analysis, were found to be 1.98 wt.%, 1.99 wt.% and 2.01 wt.%, respectively, very close to the nominal amount of 2.0 wt.%. The results (entry 5 in Table 1) clearly show that the 2.0 wt.% Pd/SO_3H-MIL–101(Cr) catalyst gives significantly higher activity and 2-methoxy-4-methylphenol selectivity as compared to the Pd/C catalyst. It should be noted that the selectivity for 2-methoxy-4-methylphenol over the prepared 2.0 wt.% Pd/SO_3H-MIL–101 catalyst is also significantly higher than that reported by Xiao et al [25] over 4.5 wt.% Pd/MSMF under the same reaction conditions with a similar conversion of vanillin (entry 6). The high selectivity over the 2.0 wt.% Pd/SO_3H-MIL–101(Cr) catalyst is probably due to the readily accessible Brønsted acidic sites distributed throughout the framework as well as an abundance of mesoporous cages of MIL–101(Cr) thus, greatly facilitating the transfer of substrates [46,47].

Table 1. Hydrodeoxygenation of vanillin over different catalysts

Entry	Catalyst	Conversion (%)	Selectivity (%)[a]	
			B	C
1[b]	MIL–101(Cr)	0	0	0
2[b]	SO_3H-MIL–101(Cr)	0	0	0
3[b]	2.0 wt.% Pd/SO_3H-MIL–101(Cr)	96.6 (100)	9.1 (0)	90.9 (100)
4[b]	2.0 wt.% Pd/MIL–101(Cr)	66.6 (86.4)	42.1 (17.9)	57.9 (82.1)
5[b]	2.0 wt.% Pd/C	55.2	78.3	21.8
6[b]	4.5 wt.% Pd/MSMF [25]	> 99.5	45.8	54.2
7[c]	5.0 wt.% Pd/SWNT-SiO_2[27]	85	53	47
8[c]	2.0 wt.% Pd/SO_3H-MIL–101(Cr)	85.4	25.6	74.4
9[d]	2.0 wt.% Pd/SO_3H-MIL–101(Cr)	100	1.6	98.4
10[d]	Pd/$CN_{0.132}$[24]	65	31	69
11[e]	2.0 wt.% Pd/SO_3H-MIL–101(Cr)	100	3.9	96.1

[a] B is the hydrogenation product, vanillin alcohol, and C is the hydrogenation/hydrogenolysis product, 2-methoxy-4-methylphenol (see Scheme 1).

[b] Reaction conditions: water, 20 ml; S/C (molar ratio of substrate to catalyst) = 200; 0.5 MPa; reaction temperature, 100 °C; reaction time, 60 min. Data in the parentheses represent reaction for 120 min.

[c] Reaction conditions: 1:1 (v/v) water/decalin, 20 ml; S/C = 100; hydrogen pressure, 0.35 MPa; reaction temperature, 100 °C; reaction time, 30 min.

[d] Reaction conditions: water, 20 ml; S/C = 350; hydrogen pressure, 1.0 MPa; reaction temperature, 90 °C; reaction time, 60 min.

[e] Reaction conditions: water, 20 ml; S/C = 1000; hydrogen pressure, 0.5 MPa; reaction temperature, 100 °C; reaction time, 300 min.

To further provide evidence in favor of the acid sites in SO_3H-MIL–101(Cr) for the hydrodeoxygenation, two control experiments were performed over 2.0 wt.% Pd/SO_3H-MIL–101(Cr) with (or without) a stoichiometric amount of pyridine with respect to the number of acid available on the MOF for the hydrogenolysis of vanillin alcohol (the intermediate in the hydrodeoxygenation of vanillin) with hydrogen. The conversion of vanillin alcohol is rather low in the presence of pyridine (Fig. S3), and this limited catalytic activity is mainly due to the poisoning of SO_3H-MIL–101(Cr) acidic active sites by the strong interaction of pyridine with the acid sites of SO_3H-MIL–101(Cr) [51,52]. This result

demonstrates the significant influence of acid active sites on the catalytic hydrodeoxygenation.

Recently, Resasco and co-workers reported that good catalytic activity and selectivity could be achieved in the hydrodeoxygenation of vanillin by depositing palladium onto SWNT-inorganic oxide hybrid (Pd/SWNT-SiO_2) in a water/oil system [27]. For example, when Pd/SWNT-SiO_2 was used as a catalyst in the two-phase system, 85% of vanillin was converted within 0.5 h with 47% selectivity for 2-methoxy-4-methylphenol (entry 7 in Table 1). For comparison, we tested the activity of the 2.0 wt.% Pd/SO_3H-MIL–101(Cr) catalyst under 30 min reaction time and obtained 85% vanillin conversion with 47% selectivity for 2-methoxy-4-methylphenol product (entry 8). Therefore, one could conclude that the nature of the support plays an important role on the activity and selectivity of the Pd catalysts for the hydrodeoxygenation of vanillin. It appears that the hydrophilic property of the 2.0 wt.% Pd/SO_3H-MIL–101(Cr) catalyst greatly affects its catalytic performance. Figure 7 shows that after the reaction, the 2.0 wt.% Pd/SO_3H-MIL–101(Cr) catalyst was well dispersed in water. In contrast to the highly aggregated state of the traditional solid catalysts, the introduction of SO_3H group increased the hydrophilic character of the 2.0 wt.% Pd/SO_3H-MIL–101(Cr) catalyst, which resulted in enhancing the catalyst dispersion in water and improving the exposure of the catalyst to the substrates (vanillin), thereby increasing the catalytic performance significantly.

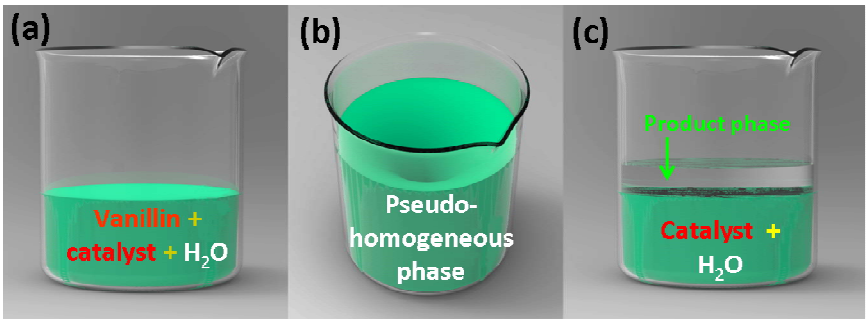

Fig. 7. Schematic representation of the catalytic hydrodeoxygenation of vanillin over the 2.0 wt.% Pd/SO_3H-MIL–101(Cr) catalyst showing photographs of (a) the reaction mixture, (b) the reaction mixture spinning using a magnetic stirrer (not shown), and (c) the product phase after the end of the reaction.

For practical applications, both high yield and low cost are required. We thus conducted the reaction with an increased vanillin/Pd (substrate/catalyst) molar ratio of S/C = 1000. Full conversion with a high 2-methoxy-4-methylphenol selectivity of 96.1% was obtained within 300 min at 100°C (entry 11 in Table 1). The high 2-methoxy-4-methylphenol yield is attributed to its poor solubility in water; once it is formed under the reaction conditions, it separates from the water phase thus avoiding further hydrogenolysis and conversion to 2-methoxyphenol (Fig. 7).

In general, transformation of the carbonyl group into a methyl group theoretically can proceed in the following three ways: (i) hydrogenation/dehydration, (ii) hydrogenation/hydrogenolysis, and (iii) direct hydrogenolysis of the C-O bond. In the present reaction, after hydrogenation, there is no H atom at the position adjacent to the hydroxyl group in vanillin alcohol, so dehydration could not take place. Therefore, the transformation of vanillin into 2-methoxy-4-methylphenol must proceed via path (ii) and/or (iii). Figure 8 shows the evolution of the product concentrations as a function of reaction time. The reaction was accompanied by a rapid increase in vanillin alcohol and a decrease in vanillin in the first 60 min, illustrating that vanillin is mainly hydrogenated to vanillin alcohol in the first step. However, even in the first 15 min, 2-methoxy-4-methylphenol was observed, suggesting that hydrogenolysis of vanillin alcohol occurred or that vanillin underwent direct hydrogenolysis of C-O as well. Xu and co-workers assumed that the direct hydrogenolysis of vanillin into 2-methoxy-4-methylphenol, without the intermediate step of hydrogenolysis of vanillin alcohol, could take place in the present of ultrafine Pd nanoparticles loaded within the cavities of MIL-101(Cr) [53]. As shown in Fig. 8, hydrogenolysis of vanillin alcohol proceeded very rapidly at longer reaction times. After 120 min, almost all of the vanillin alcohol had been converted to 2-methoxy-4-methylphenol via hydrogenolysis.

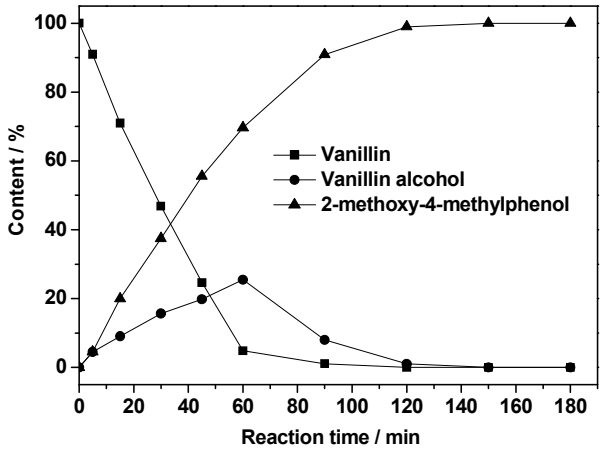

Fig. 8. Trend of reactant and product proportion as a function of reaction time over 2.0 wt.% Pd/SO_3H-MIL–101(Cr) (Reaction conditions: vanillin, 2 mmol; water, 20 ml; amount of catalyst, 50 mg; S/C = 200; hydrogen pressure, 0.5 MPa; reaction temperature, 80 °C).

In order to improve the yield of the 2-methoxy-4-methylphenol product, the reaction conditions were optimized and the results are shown in Fig. S4 and Fig. S5. It was found that under low H_2 pressure (0.2 MPa), 81.1% vanillin conversion could be achieved with 2-methoxy-4-methylphenol selectivity of 65.3% after 60 min reaction time at 100 ℃, which can be further enhanced to 100% yield of 2-methoxy-4-methylphenol under 1.0 MPa H_2 pressure (Fig. S3). Similarly, raising the temperature also led to a higher rate of vanillin conversion to 2-methoxy-4-methylphenol with a lower selectivity for vanillin alcohol (Fig. S4). These results demonstrate that the 2.0 wt.% Pd/SO_3H-MIL–101(Cr) catalyst is highly efficient for the hydrodeoxygenation of vanillin in water under mild conditions.

Furthermore, the catalyst can easily be separated from the reaction solution by simple filtration. The catalyst is highly stable and can be reused for seven cycles without losing its activity and selectivity as demonstrated in Fig. 9. The BET surface area of the spent 2.0 wt.% Pd/SO_3H-MIL–101(Cr) decreased from 820.3 to 798.7 $m^2\ g^{-1}$ (Table S1), which could be attributed to the slight trapping of residual reactants or products inside the SO_3H-MIL–101(Cr) pores. In addition, we measured the XRD pattern of the spent catalysts and found the crystalline structure of the SO_3H-MIL–101(Cr) was still maintained after the

seventh cycle (pattern d in Fig. 1). TEM images of the used 2.0 wt.% Pd/SO_3H-MIL–101(Cr) catalysts only show slight aggregation of the Pd nanoparticles (Fig.S6), which does not affect the activity of the catalysts within the seven cycles. Moreover, the concentration of Pd in the reaction solution was determined by ICP-AES to be < 0.1 ppm, indicating that leaching of Pd into the solvent is negligible.

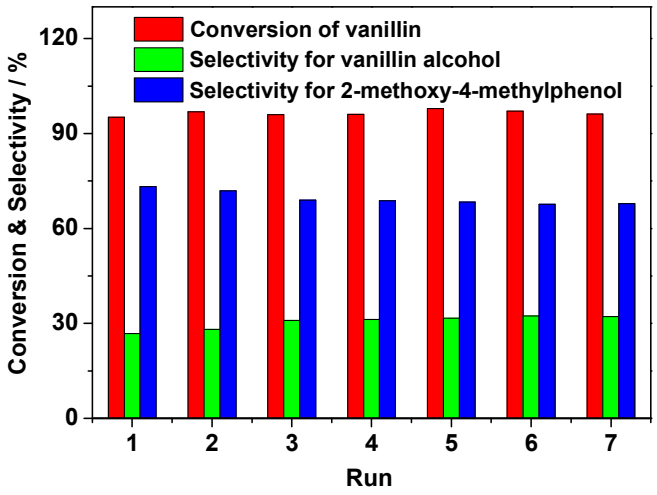

Fig. 9. Reusability of 2.0 wt.% Pd/SO_3H-MIL–101(Cr) in the catalytic hydrodeoxygenation of vanillin (Reaction conditions: vanillin, 2 mmol; water, 20 ml; amount of catalyst, 50 mg; hydrogen pressure, S/C = 200; 0.5 MPa; reaction temperature, 80 °C; reaction time, 60 min).

4. Conclusions

In conclusion, we have developed a heterogeneous tandem catalyst for the hydrodeoxygenation of vanillin, a common component in lignin-derived bio-oil, under mild reaction conditions. The developed 2.0 wt.% Pd/SO_3H-MIL–101(Cr) catalyst exhibits high catalytic activity and selectivity in the tandem hydrogenation-deoxygenation reactions and can be reused seven times without any loss in activity and selectivity. The high catalytic performance for Pd/SO_3H-MIL–101(Cr) is attributed to the unique characteristics of the SO_3H-MIL–101(Cr) support, which leads not only to very stable and uniform dispersion of

the Pd nanoparticles but also to possible electronic activation of the reactants and good dispersion of the catalyst in water. This 2.0 wt.% Pd/SO_3H-MIL–101(Cr) catalyst holds promising potential for the biofuel upgrade process.

Acknowledgements

This project was supported by the Zhejiang Provincial Natural Science Foundation of China (LY13B030002) and the National Natural Science Foundation of China (21303166, 20806075).

References

1. NAS-NAE-NRC (National Academy of Sciences-National Academy of Engineering-National Research Council), America's Energy Future: Technology and Transformation. Washington, D.C. The National Academies Press **2009**.

2. D. Cahen and I. Lubomirsky, *Mat. Today* 2008, 11, 16–20.

3. H. Olcay, A. V. Subrahmanyam, R. Xing, J. Lajoie, J. A. Dumesic and G. W. Huber, *Energy Environ. Sci*., 2013, 6, 205–216.

4. C. B. Field, J. E. Campbell, D. B. Lobell, *Biomass energy: The scale of the Potential Resource. Trends in Ecology and Evolution* 2008, 23, 65–72.

5. E. Butler, G. Devlin, D. Meier and K. McDonnell, *Renew. Sustainable Energy Rev*., 2011, 15, 4171–4186.

6. T. H. Parsell, B. C. Owen, I. Klein, T. M. Jarrell, C. L. Marcum, L. J. Haupert, L. M. Amundson, H. I. Kenttamaa, F. Ribeiro, J. T. Miller and M. M. Abu-Omar, *Chem. Sci*., 2013, 4, 806–813.

7. D. Fengel and G. Wegener, *Wood: Chemistry, Ultrastructure, Reactions.* Berlin; New York: de Gruyter, 1989, pp 1–613.

8. I. Graca, J. M. Lopes, H. S. Cerqueira and M. F. Ribeiro, *Ind. Eng. Chem. Res*., 2013, 52, 275–287.

9. C. Zhao, Y. Kou, A. A. Lemonidou, X. B. Li and J. A. Lercher, *Angew. Chem., Int. Ed*., 2009, 48, 3987–3990.

10. J. Y. He, C. Zhao and J. A. Lercher, *J. Am. Chem. Soc*., 2012, 134, 20768–20775.

11. D. M. Alonso, S. G. Wettstein and J. A. Dumesic, *Chem. Soc. Rev*., 2012, 41, 8075–8098.

12. P. Gallezot, *Chem. Soc. Rev.*, 2012, 41, 1538–1558.

13. S. De, B. Saha and R. Luque, *Bioresour. Technol.*, 2015, 178, 108–118.

14. M. Saidi, F. Samimi, D. Karimipourfard, T. Nimmanwudipong, B. C. Gates and M. R. Rahimpour, *Energy Environ. Sci.*, 2014, 7, 103–129.

15. A. H. Zacher, M. V. Olarte, D. M. Santosa, D. C. Elliott and S. B. Jones, *Green Chem.*, 2014, 16, 491–515.

16. J. Yang, C. L. Williams, A. Ramasubramaniam and P. J. Dauenhauer, *Green Chem.*, 2014, 16, 675–682.

17. T. P. Vispute, H. Zhang, A. Sanna, R. Xiao and G. W. Huber, *Science*, 2010, 330, 1222–1227.

18. G. W. Huber, J. N. Chheda, C. J. Barrett and J. A. Dumesic, *Science*, 2005, 308, 1446–1450.

19. X. Huang, C. Guo, J. Zuo, N. Zheng and G. D. Stucky, *Small*, 2009, 5, 361–365.

20. K. Yoon, Y. Yang, P. Lu, D. Wan, H. C. Peng, K. Stamm Masias, P. T. Fanson, C. T. Campbell and Y. Xia, *Angew. Chem. Int. Ed*., 2012, 51, 9543–9546.

21. S. H. Joo, J. Y. Park, C. K. Tsung, Y. Yamada, P. Yang and G. A. Somorjai, *Nat. Mater*., 2009, 8, 126–131.

22. X. Yang, Y. Liang, X. Zhao, Y. Song, L. Hu, X. Wang, Z. Wang and J. Qiu, *RSC Adv*., 2014, 4, 31932–31936.

23. A. La Torre, M. d. C. Giménez-López, M. W. Fay, G. A. Rance, W. A. Solomonsz, T. W. Chamberlain, P. D. Brown and A. N. Khlobystov, *ACS Nano*, 2012, 6, 2000–2007.

24. X. Xu, Y. Li, Y. Gong, P. Zhang, H. Li and Y. Wang, *J. Am. Chem. Soc.*, 2012, 134, 16987–16990.

25. Z. Lv, Q. Sun, X. Meng and F. S. Xiao, *J. Mater. Chem. A*, 2013, 1, 8630–8635.

26. Z. Zhu, H. Tan, J. Wang, S. Yu and K. Zhou, *Green Chem.*, 2014, 16, 2636–2643.

27. S. Crossley, J. Faria, M. Shen and D. E. Resasco, *Science*, 2010, 327, 68–72.

28. O. M. Yaghi, M. O'Keeffe, N. W. Ockwig, H. K. Chae, M. Eddaoudi and J. Kim, *Nature*, 2003, 423, 705–714.

29. N. Stock and S. Biswas, *Chem. Rev.*, 2012, 112, 933–969.

30. S. Kitagawa, R. Kitaura and S. Noro, *Angew. Chem. Int. Ed.*, 2004, 43, 2334–2375.

31. M. P. Suh, H. J. Park, T. K. Prasad and D. W. Lim, *Chem. Rev.*, 2012, 112, 782–835.

32. J. R. Li, J. Sculley and H. C. Zhou, *Chem. Rev.*, 2012, 112, 869–932.

33. G. Férey, C. Mellot-Draznieks, C. Serre, F. Millange, J. Dutour, S. Surble and I. Margiolaki, *Science*, 2005, 309, 2040–2042.

34. G. Akiyama, R. Matsuda, H. Sato, M. Takata and S. Kitagawa, *Adv. Mater.*, 2011, 23, 3294–3297.

35. L. Lu, X. Y. Li, X. Q. Liu, Z. M. Wang and L. B. Sun, *J. Mater. Chem. A*, 2015, 3, 6998–7005.

36. H. Liu, L. Chang, L. Chen and Y. Li, *J. Mater. Chem. A*, 2015, 3, 8028–8033.

37. S. J. Bao, R. Krishna, Y. B. He, J. S. Qin, Z. M. Su, S. L. Li, W. Xie, D. Y. Du, W. W. He, S. R. Zhang and Y. Q. Lan, *J. Mater. Chem. A*, 2015, 3, 7361–7367.

38. H. Yu, J. Xie, Y. Zhong, F. Zhang and W. Zhu, *Catal. Commun.*, 2012, 29, 101–104.

39. E. V. Ramos-Fernandez, C. Pieters, B. van der Linden, J. Juan-Alcaniz, P. Serra-Crespo, M. W. G. M. Verhoeven, H. Niemantsverdriet, J. Gascon and F. Kapteijn, *J. Catal.*, 2012, 289, 42–52.

40. A. Klinkebiel, N. Reimer, M. Lammert, N. Stock and U. Luning, *Chem. Commun.*, 2014, 50, 9306–9308.

41. X. Zhao, Y. Jin, F. Zhang, Y. Zhong and W. Zhu, *Chem. Eng. J.*, 2014, 239, 33–41.

42. A. S. Khder, H. M. A. Hassan and M. S. El-Shall, *Appl. Catal. A.*, 2014, 487, 110–118.

43. M. S. El-Shall, V. Abdelsayed, A. Khder, H. M. A. Hassan, H. M. El-Kaderi and T. E. Reich, *J. Mater. Chem.*, 2009, 19, 7625–7631.

44. B. Li, K. Leng, Y. Zhang, J. J. Dynes, J. Wang, Y. Hu, D. Ma, Z. Shi, L. Zhu, D. Zhang, Y. Sun, M. Chrzanowski and S. Ma, *J. Am. Chem. Soc.*, 2015, 137, 4243–4248.

45. F. Zhang, Y. Jin, J. Shi, Y. Zhong, W. Zhu, and M. S. El-Shall, *Chem. Eng. J.*, 2015, 269, 236-244.

46. Y. Zang, J. Shi, F. Zhang, Y. Zhong and W. Zhu, *Catal. Sci. Technol.*, 2013, 3, 2044–2049.

47. Y. Jin, J. Shi, F. Zhang, Y. Zhong and W. Zhu, *J. Mol. Catal. A,* 2014, 383–384, 167–171.

48. P. Kusgens, M. Rose, I. Senkovska, H. Frode, A. Henschel, S. Siegle, S. Kaskel, *Microporous Mesoporous Mat*. 2009, 120, 325–330.

49. H. Liu, T. Jiang, B. Han, S. Liang and Y. Zhou, *Science*, 2009, 326, 1250–1252.

50. M. Rueping, R. M. Koenigs and I. Atodiresei, *Chem. Eur. J.* ***2010,*** 16, 9350–9365.

51. Y. Z. Chen, Y.X. Zhou, H. Wang, J. Lu, T. Uchida, Q. Xu, S.H. Yu and H.L. Jiang, *ACS Catal.*, 2015, 5, 2062–2069.

52. F. Zhang, J. Shi, Y. Jin, Y. Fu, Y. Zhong and W. Zhu, *Chem. Eng. J.*, 2015, 259, 183–190.

53. A. Aijaz, Q. L. Zhu, N. Tsumori, T. Akita and Q. Xu, *Chem. Commun*., 2015, 51, 2577–2580.

Graphical abstract

The developed Pd/SO_3H-MIL–101(Cr) catalyst exhibits novel synergy in hydrodeoxygenation of vanillin at low H_2 pressure under mild conditions.